

Total Electron Content Fluctuations and Their Implications for GPS Signal Delay over Thailand: Insights from Low Latitudes during the Ascending Phase of Solar Cycle 25

Thanapon Keokhumcheng¹, Prarinya Phothila², Samatchaya Maichuen², Nitipat Buakao², Jianfeng Zhang², Prasert Kenpankho^{*,2}

⁽¹⁾ Institute of Vocational Education, Department of Electronics, Nongbualumphu Technical College, Nongbualumphu, Thailand

⁽²⁾ King Mongkut's Institute of Technology Ladkrabang, Department of Engineering Education, School of Industrial Education and Technology, Bangkok, Thailand

Article history: received October 01, 2025; accepted April 18, 2026

Abstract

This research investigates how fluctuations in Total Electron Content (TEC) on the global positioning system (GPS) affect GPS performance in Thailand's low latitude region during the ascending phase of solar activity 25th, utilizing data from 2023 to 2025. To capture TEC variations, five GPS monitoring stations were strategically deployed along a north-south transect across Thailand including Bangkok station, Chiang Mai station, KMITL Chumphon station, Nongbualumphu station, and Phuket station. TEC data collected from these stations were analyzed using statistical techniques with comparisons to IGS and IRI models to explore ionospheric dynamics and solar activity throughout the ascending phase of the cycle years, influencing TEC values and the time delay in the navigation system. The research reveals how solar-induced ionospheric changes influence TEC levels and cause time delays in GPS signals, which are critical factors for satellite navigation accuracy. These insights pave the way for enhancing GPS reliability and efficiency in low latitude regions, contributing to the development of more robust global navigation systems.

Keywords: Total Electron Content; Solar Activity; Solar 25th Cycle; Time Delay; Low Latitude Region

1. Introduction

Global Positioning System (GPS) satellites transmit signals essential for positioning, navigation, and timing. However, these signals are significantly affected by ionospheric Total Electron Content (TEC), which introduces delays and reduces positioning accuracy (Keokhumcheng and Kenpankho, 2025). TEC variations are primarily driven by solar activity, particularly fluctuations in sunspot numbers that alter ionospheric electron density. This study focuses on Solar cycle 25, which began in late 2019 and reached its peak in August 2024 with a monthly

median F10.7 cm flux of 219.6 sfu. The current 25th solar cycle began in 2020 and is expected to reach its maximum in August 2024, as indicated by the monthly median F10.7 cm radio flux shown in Table 1. It has been projected to exhibit stronger solar activity compared to Solar Cycle 24 (Javaraiah, 2024). Solar flux measurements, such as the F10.7 cm index from Space Weather Canada, provide reliable indicators of solar activity and its influence on ionospheric electron content. This study focuses on the low-latitude region above Thailand, where ionospheric irregularities are particularly pronounced. TEC data were obtained from five multi-frequency BG2s GPS receivers deployed across Thailand from 2023 to 2025. Observed TEC values were statistically analyzed and converted into GPS signal time delays to quantify the impact on navigation accuracy. Comparisons with the International GNSS Service (IGS) and the International Reference Ionosphere (IRI-2016) model were performed only as a climatological background reference, not as a direct evaluation of model performance. Correlation coefficients between measured and modeled TEC were calculated to quantify the model's accuracy and reliability, while also providing contextual understanding of ionospheric behavior during the ascending phase of Solar cycle 25. The results provide insights into the relationship between solar activity, TEC variations, and GPS signal time delays, contributing to the development of improved compensation techniques for reliable satellite-based navigation in low-latitude regions.

A literature review of publications published between 1990 to 2025 was performed. These works offer a theoretical and methodological framework for the current study and are summarized. Blewitt (1990) conducted a study on Turbo Edit, an automatic GPS data editing algorithm designed to detect and correct outliers and cycle slips in undifferenced dual-frequency carrier phase measurements. Validation using a large dataset demonstrated that analyst intervention was needed in only 1% of cases, and the algorithm is now being adapted for real-time applications. In 2003, Ma and Maruyama (2003) developed a method to derive ionospheric TEC and estimate instrumental biases of GPS satellites and receivers using Japan's dense GEONET network. The method divided the ionosphere into spatial meshes and applied least-squares fitting to solve for TEC and bias values, showing stable biases and good agreement with ionospheric critical frequency data. In 2011, Kenpankho et al. (2011) evaluated GPS TEC over Chumphon, Thailand, using data from 2004 to 2006. Their findings revealed that the IRI-2007 model consistently underestimated TEC values, whereas the IGS TEC data showed significantly better agreement with the observations. In 2015, Chowdhary et al. (2015) analyzed TEC variations over equatorial anomaly regions in Thailand using dual-frequency GPS data, identifying diurnal, monthly, and seasonal patterns correlated with solar activity, and noted model limitations during geomagnetic storms. In 2016, Jesus et al. (2016) investigated the ionospheric responses to the intense geomagnetic storm of late September 2012 over the Americas and Africa, revealing F-region uplift and both positive and negative TEC storm effects linked to atmospheric wind and composition changes. In 2022, Bilitza et al. (2022) reviewed the International Reference Ionosphere (IRI) project and model. IRI is recognized as the official standard for the Earth's ionosphere by the International Standardization Organization, the International Union of Radio Science, the Committee on Space Research, and the European Cooperation for Space Standardization. Mengistu et al. (2019) evaluated the IRI-2016 model's performance in simulating vertical TEC over East Africa, showing under- and over-estimations depending on conditions and poor reproduction of geomagnetic storm effects. In 2020, Tsidu and Zegeye (2020) compared IRI-2016 TEC with global GPS observations during solar minimum and maximum, finding better accuracy during solar minimum but with limitations related to seasonality and spatial coverage. In 2021, Oyedokun et al. (2021) studied TEC responses to intense geomagnetic storms during solar cycle 24 maximum over African equatorial stations, observing storm-phase-dependent TEC changes and poleward expansion of the Equatorial Ionization Anomaly (EIA). Singh et al. (2021) analyzed low-latitude TEC variations during four intense storms in solar cycle 24 in India, relating changes to local time, storm winds, thermosphere composition, and interplanetary electric fields. Akala et al. (2021) investigated the solar origins of a weak geomagnetic storm in August 2018 and its weak prompt penetration electric field effects, which confined plasma density within $\pm 15^\circ$ magnetic latitude in the EIA region, exhibiting hemispheric asymmetry. Arowolo et al. (2021) examined eight intense geomagnetic storms' interplanetary sources and effects on African TEC, distinguishing impacts from ICME and CIR storms with different TEC response patterns. In 2022, Brajša et al. (2022) applied the Minimum-Maximum precursor method to predict Solar cycle 25's sunspot maximum, suggesting it would be comparable or lower than Cycle 24, consistent with a declining solar activity trend. Du (2022) analyzed correlations between sunspot numbers and hemispheric solar cycle amplitudes, predicting northern and southern hemisphere maxima around late 2023 and mid-2024, respectively. Ogwala et al. (2022) investigated longitudinal TEC variations in equatorial regions, revealing a decreasing trend and regional differences not captured well by current ionospheric models. In 2023, Lozitsky and Efimenko (2023) forecasted a moderate Solar cycle 25 amplitude without a long-term minimum transition. Nagovitsyn

and Ivanov (2023) proposed a high correlation between sunspot numbers before solar minimum and subsequent maxima, predicting the Cycle 25 peak in late 2023 to early 2024. Kalkan et al. (2023) used a NARX neural network trained on multi-indicator data to predict Solar cycle 25 maximum in early 2025 with good accuracy. Keokhumcheng and Kenpankho (2025) validated single-frequency GPS TEC measurements in Thailand, confirming their reliability for ionospheric studies in low latitudes where dual-frequency data are unavailable. Ansari et al. (2024) explored plasma bubble effects on GPS position accuracy in Southeast Asia by implementing wavelet transformation methods to alleviate signal disturbance. Their results showed greater positioning stability in disturbed ionospheric conditions, emphasizing the role of sophisticated signal processing techniques as GNSS for use in equatorial areas. Building on this, Ansari et al. (2025) studied multi-constellation GNSS signal ionospheric gradients in a UAV operating over Thailand with Global Ionospheric Maps (GIM) and the Klobuchar model. This research led to the identification of localized ionospheric gradients, which highlighted the necessity of robust correction models to support navigation by UAVs and similar GNSS-dependent operations in Southeast Asia.

Recent studies focusing on the impact of TEC changes on GPS performance, particularly at low latitudes during the Solar cycle 25, have been instrumental in shaping this research methodology. They draw on the work of Keokhumcheng and Kenpankho (2025), who demonstrated that single-frequency receivers can reliably estimate TEC, providing a practical approach for monitoring ionospheric fluctuations. Additionally, Kenpankho et al. (2011) revealed that while the IRI-2007 model tends to underestimate TEC at the Chumphon station, IGS TEC aligns more closely with observed data, highlighting the limitations of global empirical models in equatorial regions. The researchers studied GPS receiver bias estimation at Chumphon station and discovered that Lagrange interpolation provided faster, more accurate results than existing methods. Bilitza et al. (2022) further recognized the IRI model as the internationally endorsed standard approved by ISO, URSI, COSPAR, and ECCS and described its continuous improvements, yet noted remaining accuracy challenges over equatorial latitudes. These insights collectively inform and justify the present study's focus on localized TEC analysis over Thailand during 2022-2024 to better understand TEC fluctuations and their implications for GPS performance during the ascending phase of Solar cycle 25 (2023-2025).

In the course of this study, variations in TEC were examined to evaluate GPS signal delays in the low-latitude region of Thailand. TEC measurements from 5 GPS stations during Solar cycle 25 (2023-2025) were compared with IRI model predictions, and correlation coefficients were computed to assess model performance. TEC data from multi-frequency BG2s GPS receivers were analyzed alongside solar activity indices to evaluate their effect on ionospheric time delays impacting GPS signals. The results reveal substantial relationships between TEC variability and solar activity levels, demonstrating the significant impact of heightened solar activity on satellite signal delay in the region. These findings deepen our understanding of ionospheric dynamics and provide potential pathways for improving GPS accuracy and reliability in navigation and communication applications across Thailand and similar low-latitude environments.

2. Data and Methodology

This study utilizes data related to TEC, which quantifies the integrated number of free electrons along the signal path between GPS satellites and ground receivers. TEC data serve as a key indicator for increasing ionospheric conditions that affect satellite signal propagation. Solar activity parameters, including sunspot number, solar flux, and geomagnetic indices, are incorporated to capture variations in solar output that influence ionospheric electron density. Focusing on the Solar 25th Cycle, which commenced around 2019-2020, we focus on 2023-2025, and it is characterized by increasing solar activity. The analysis targets the ascending phase, where ionospheric variability tends to intensify in 2023-2025. The study also investigates the time delay between solar activity indicators and the corresponding response in TEC, an important factor for modeling ionospheric dynamics and improving GPS correction algorithms. Given the unique ionospheric behavior in the low-latitude region above Thailand, including phenomena such as the equatorial ionization anomaly, this research specifically analyzes TEC fluctuations in this geographic zone. GPS receiver data spanning the period 2023-2025 are processed to extract TEC variations, which are then correlated with solar and sunspots in Solar cycle 25 (2023-2025) indices to indicate the underlying relationships and time-dependent responses. The methodology involves preprocessing of raw GPS data, applying calibration and bias correction, followed by statistical and time-series analysis to quantify TEC variability and assess the impact of solar activity during the Solar 25th Cycle's ascending phase in the low-latitude environment.

2.1 Low Latitude Region

Geographic areas near the Earth’s magnetic equator, such as Thailand, are characterized by unique ionospheric behaviors, including the equatorial ionization anomaly and irregular plasma structures that cause complex TEC variations. Therefore, Thailand can use its geography to set up a GPS satellite receiving station to study TEC from the ionosphere caused by sunspots during the 24th-25th solar activity period. By distributing multi-frequency GPS satellite receiving stations called BG2s, which have been installed throughout Thailand, covering the entire country, a total of five stations are shown in Fig. 1.

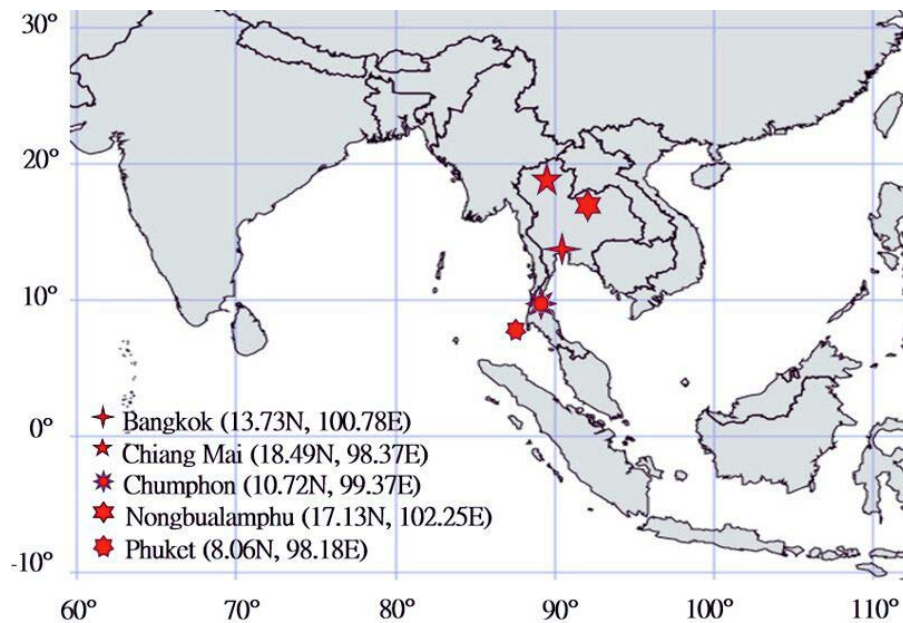


Figure 1. Installation location of the BG2s satellite receiver in Thailand.

Figure 1 consists of Bangkok at the King Mongkut Institute of Technology Ladkrabang (SIET KMITL), the coordinates: 13.73N, 100.78E, Chiang Mai at Mae Jam (MMAI), the coordinates: 18.49N, 98.37E, Chumphon (KMITL Chumphon), the coordinates: 10.72N, 99.37E, Nongbualumphu (NBUA), the coordinates: 17.13N, 102.25E, and Phuket (PKET), the coordinates: 8.06N, 98.18E, respectively.

2.2 Solar Activity and Solar 25th Cycle

Solar cycle 25 began in December 2019 and is expected to last until 2030-2031. During its ascending phase (2020-mid 2024), solar activity increased steadily, marked by increasing sunspot numbers, solar flares, and coronal mass ejections. The cycle reached its peak in August 2024, with F10.7 values recorded at 219.6 sfu, before entering an early declining phase in 2025. Thus, the interval 2023-2025 cannot be described solely as “increasing”; instead, it encompasses the late ascending phase, the peak, and the beginning of the decline. Early data suggest that this cycle may exceed initial activity predictions, presenting challenges for GPS reliability and ionospheric modeling. To better characterize the long-term evolution of Solar cycle 25, data from earlier years (2020-2023) are included to define the ascending phase more accurately.

The F10.7 cm monthly median (2020-2025) provide a comprehensive record of solar activity, serving as a key reference for space weather, ionospheric research, and solar-terrestrial studies. The current 25th cycle, starting in 2020 and peaking in mid-2025, is projected by Javaraiah (2024) to be stronger than Cycle 24. Solar flux measurements, particularly F10.7 cm from Space Weather Canada (SWC), serve as reliable solar activity indicators correlating with TEC levels. In this study, values exceeding 150 sfu are defined as high solar activity, consistent with the threshold applied in Fig. 2.

TEC Fluctuations and Their Implications for GPS

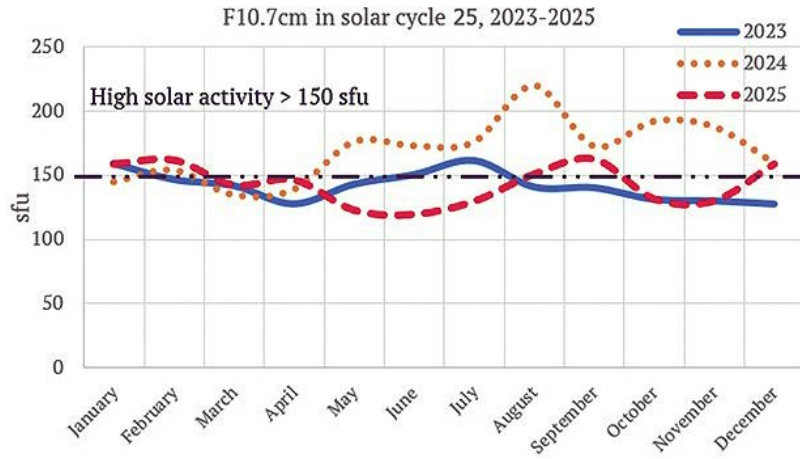


Figure 2. The F10.7 index in Solar cycle 25 during the years 2023-2025.

Figure 2 illustrates the F10.7 cm radio flux (sfu) from 2023 to 2025. Values exceeding 150 sfu are defined as high solar activity. Values were then averaged to obtain the monthly median F10.7 cm, which is summarized by year in Table 1.

Table 1. Monthly median F10.7 cm radio flux (Solar cycle 25).

F10.7 cm radio flux (sfu)			
Month/Year	2023	2024	2025
January	159.20	144.90	158.40
February	146.60	153.90	161.50
March	141.80	134.70	142.20
April	127.40	138.95	146.40
May	142.90	175.90	123.10
June	150.45	172.80	119.80
July	161.60	175.70	129.80
August	140.75	219.60	150.60
September	140.15	172.45	162.25
October	131.00	191.80	131.70
November	129.80	187.50	130.20
December	127.30	159.40	158.40

Table 1 presents the monthly median values of the F10.7 cm radio flux from January 2023 to December 2025. In 2023, the values ranged from 127.30 sfu (December) to 161.60 sfu (July), with most months fluctuating between 130 and 160 sfu. In 2024, solar activity markedly increased, reaching a maximum of 219.60 sfu in August and a minimum of 134.70 sfu in March. In contrast, the values in 2025 indicate a gradual decline following the 2024 peak. The year began with relatively high flux levels (158.40 sfu in January and 161.50 sfu in February) but decreased to the lowest value of 119.80 sfu in June. A modest recovery was observed in July (129.80 sfu) and subsequent months, with September reaching 162.25 sfu, before stabilizing around 130-158 sfu toward the end of the year. These results confirm that solar activity peaked in mid-2024 and then weakened during 2025.

2.3 Total Electron Content (TEC)

TEC represents the total number of free electrons integrated along the signal path between GPS satellites and ground-based receivers. Expressed in TEC units (1 TECU = 10^{16} electrons/m²), TEC provides a fundamental measure of ionospheric conditions that directly influence the propagation speed and accuracy of satellite signals. Variations in TEC, driven primarily by solar and geomagnetic activity, can induce significant fluctuations in radio signal travel times, thereby affecting the precision of GPS-based positioning and navigation. Dual-frequency GPS receivers enable TEC estimation by analyzing signal delays at two distinct carrier frequencies, allowing correction of ionospheric errors. Following Blewitt (1990), Slant TEC (STEC) is measured along the line-of-sight to the satellite, while Vertical TEC (VTEC) provides a generalized measure of ionospheric electron density. Monitoring VTEC is particularly important during Solar cycle 25, especially in the period 2023-2025, which encompasses the late ascending phases, peak, and early declining phases. Enhanced solar activity during this interval significantly increases ionospheric electron density and amplifies GPS signal delays. Accurate TEC measurements are therefore essential for assessing space weather impacts on GPS signals and for improving navigation, communication, and early warning systems. By analyzing TEC variations across multiple GPS stations in Thailand, this study provides insights into the regional ionospheric response to solar activity, helping to characterize both temporal and spatial fluctuations in electron content during (2023-2025).

Specifically, GPS satellites transmit signals at two distinct frequencies, and as these signals pass through the ionosphere, they experience different delays due to electron density along the path. By comparing the timing differences between these dual-frequency signals, it is possible to derive the slant TEC (STEC), which represents the electron content along the oblique satellite-to-receiver line of sight. Mathematically, the STEC from a satellite to a receiver can be obtained from the difference between the pseudoranges (P1 and P2) and the difference between the phases (L1 and L2) of the two frequencies by Blewitt (1990) shown as Eq. (1) and (2).

$$STEC_p = \frac{2(f_1 f_2)^2}{k(f_1^2 - f_2^2)} (P_2 - P_1) + \tau^r + \tau^s \quad (1)$$

$$STEC_L = \frac{2(f_1 f_2)^2}{k(f_1^2 - f_2^2)} (L_1 \lambda_1 - L_2 \lambda_2) + \varepsilon^r + \varepsilon^s \quad (2)$$

whereas

k is related to the ionosphere refraction, is $80.62 \text{ (m}^3/\text{s}^2)$,

P_1, P_2 are the pseudoranges of the two GPS signals,

f_1, f_2 are denoted by the frequencies of the two GPS signals, while

L_1, L_2 are carrier phases and

λ_1, λ_2 are wavelength,

τ^r, ε^r are biases in code measurements are typically expressed with respect to the P1 and P2 pseudorange signals,

τ^s, ε^s are Biases across different frequencies are expressed in terms of both pseudorange signals (P1, P2) and carrier phase data (L1, L2).

Since STEC is measured along an inclined path, it is often necessary to convert it to vertical TEC (VTEC) for consistency in ionospheric studies. This conversion employs a mapping function that accounts for the satellite elevation angle and assumes a fixed height for the ionospheric shell, commonly set at 400 km altitude by

TEC Fluctuations and Their Implications for GPS

Kenpankho et al. (2011). The vertical TEC is then obtained by adjusting the STEC with the cosine of the zenith angle at the ionospheric shell, calculated from VTEC by Keokhumcheng and Kenpankho (2025), Ma and Maruyama (2003), and Kenpankho et al. (2011). TEC can be obtained using Eq. (3).

$$VTEC = STEC \times \cos \chi \quad (3)$$

Here, χ is the angle of the zenith satellite receiver as

$$\chi = \arcsin\left(\frac{R_E \cos \alpha}{R_E + h}\right)$$

whereas α is the satellite elevation angle, R_E is the radius of Earth, and h is the ionosphere layer.

In general, the STEC calculated from the carrier wave phase has less noise than that from Eq. (2). However, ambiguity in the integer values of the phases (L), known as the shift, often occurs. This shift can generally be corrected by using pseudo-distance difference information to obtain the VTEC by Kenpankho et al. (2011) as in Eq. (4).

$$VTEC = (STEC - b_s - b_r) \times \cos \chi \quad (4)$$

where b_s and b_r are the estimated satellite and receiver biases. Satellite error data is obtained from the Earthquake Monitoring Division, Thai Meteorological Department (Thailand), in conjunction with the Space, Satellite, and Study Laboratory (SSS Lab), Department of Engineering Education, School of Industrial Education and Technology, King Mongkut's Institute of Technology Ladkrabang, Bangkok. This data is based on GPS and BGS2 receivers manufactured by the Institute of Geology and Geophysics, Chinese Academy of Sciences (IGGCAS) of China. Currently, there are more than 20 GPS receiver stations distributed throughout Thailand.

The overall procedure for calculating VTEC from GPS receiver data can be outlined as follows this method models VTEC using polynomial functions that approximate ionospheric variations. Describes ionospheric pierce point coordinates based on angular geometry involving satellite-receiver positions and the thin-shell ionosphere altitude. In this framework, STEC is approximated by a polynomial in the angular coordinate variations, as proposed by Kenpankho et al. (2021), as shown in Eq. (5).

$$STEC_u^m(n) = o_u^m + M(\epsilon_m(n))(c_1 + c_2\bar{\phi}_p + c_3\bar{\theta}_p + c_4\bar{\phi}_p^2 + c_5\bar{\phi}_p\bar{\theta}_p + c_6\bar{\theta}_p^2) \quad (5)$$

Whereas o_u^m represents the combined biases of the satellite and receiver, with subscripts denoting the receiver and superscripts indicating the satellite. The function $(\epsilon_m(n))$ is derived from satellite-receiver geometry using ephemeris data. Longitude ($\bar{\phi}_p$) and latitude ($\bar{\theta}_p$) define the spatial coordinates, while coefficients c_i , $i = 1, \dots, 6$ construct the polynomial representation of VTEC. Once STEC is determined, VTEC is obtained via the thin-shell approximation of the Single Layer Ionosphere Model.

With STEC available, VTEC is evaluated by applying the thin-shell geometry of the Single Layer Ionosphere Model by Kenpankho et al. (2021) as in Eq. (6).

$$VTEC_u^m(n) = \frac{STEC_u^m(n)}{M(\epsilon_m(n))} \quad (6)$$

$M(\epsilon_m(n))$ represents the mapping is

$$M(\epsilon_m(n)) = \left[1 - \left(\frac{R \cos \lambda(n)}{R + h}\right)^2\right]^{-1/2}, \quad (7)$$

where λ denotes the satellite elevation angle, R corresponds to the Earth's radius (6378.137 km), and h represents the ionospheric shell height of 428.8 km (Kenpankho et al., 2021).

The coefficients of the polynomial together with offset values are derived via least-squares fitting, carried out separately for daytime and nighttime data sets. Ephemeris and bias information for satellites are widely available in IONEX products from IGS. For every satellite and time index within two hours, Eq. (5) is established. For example, for satellite M_1 at time index N_1 , the equation is given by Kenpankho et al. (2021) as Eq. (8).

$$STEC_u^{m_1}(n_1) = o_u^{m_1} + M(\epsilon_m(n_1)) \left(VTEC_u^{m_1}(n_1) \right) \quad (8)$$

where

$$VTEC_u^{m_1}(n_1) = c_1 + c_2 \bar{\phi}_p^{m_1}(n_1) + c_3 \bar{\theta}_p^{m_1}(n_1) + c_4 [\bar{\phi}_p^{m_1}(n_1)]^2 + c_5 \bar{\phi}_p^{m_1}(n_1) \bar{\theta}_p^{m_1}(n_1) + c_6 [\bar{\theta}_p^{m_1}(n_1)]^2$$

Eq. (8), when applied to M_t satellites and N_t measurement samples, produces $M_t \times N_t$ equations for a given session. The unknown total bias o_u^m and coefficients $c_1, c_2, c_3, c_4, c_5, c_6$ are determined using least-squares approximation. Because each satellite has a distinct bias, the RINEX-provided satellite biases are subtracted from the median values to obtain receiver bias estimates. A single daily receiver bias is then derived by taking the median across all 24-hour measurements. From this perspective, VTEC is simply TEC. Once the TEC value is obtained from the GPS signal, it is called TEC.

2.4 Time delay

The 25th Solar cycle (Cycle 25), which began in December 2019, is expected to last about 11 years. During its ascending phase, increased solar activity marked by rising sunspot numbers, solar flares, and coronal mass ejections has led to greater ionospheric variability and significant TEC fluctuations. Early observations indicate activity levels exceeding forecasts, raising concerns for GPS signal reliability. Moreover, a time delay often exists between solar activity changes and ionospheric responses, due to complex energy transfer processes. Accurately accounting for this delay is essential to minimizing GPS positioning errors and enhancing space weather prediction models.

The time delay of GPS signals is primarily associated with their propagation through the Earth's atmosphere before reaching ground-based receivers. A significant portion of this delay arises when the signals traverse the ionosphere, which is a dispersive medium characterized by a high and temporally varying concentration of free electrons. Raw GPS measurements can be used to derive the TEC, which quantifies the integrated electron density along the signal path. TEC values are then applied to compute the ionospheric delay. Variations in the electron density directly influence the velocity of GPS signal propagation, thereby introducing a time delay along the signal path. This ionospheric delay is one of the major sources of error in satellite-based navigation and positioning systems and must be carefully modeled or corrected to ensure the accuracy and reliability of GPS-derived measurements (Kenpankho et al., 2011). In the study of signal delay in Global Navigation Satellite System (GNSS) transmissions, the investigation can be initiated by considering the fundamental propagation delay that occurs when signals pass through a general medium (Davies and Liu, 1991). This delay can be expressed mathematically as follows, Eq. (9).

$$\Delta t = \left[\frac{40.3}{c} \times \frac{TEC}{f^2} \right] \quad (9)$$

where

Δt is the signal delay, expressed in seconds (s)

c is the speed of light, equal to 299,792,458 meters per second (m/s);

TEC is the TEC along the signal path Thus, the GPS time delay can be calculated by Eq. (10).

$$\Delta t = 3.5023 \times 10^{-26} TEC \quad (10)$$

2.5 Median as a Measure of Central Tendency

The median is a positional measure of central tendency that divides an ordered dataset into two halves. It corresponds to the 50th percentile and is particularly robust against extreme values or outliers, making it suitable for geophysical datasets that often exhibit skewed distributions (e.g., seismic travel times, geomagnetic measurements).

For data presented in frequency tables, the median can be approximated using the method of Hogg et al. (2005).

$$Median = L + \left(\frac{\frac{n}{2} - CF}{f} \right) \cdot h \quad (11)$$

where:

- L is the lower boundary of the median class
- n is the total number of observations
- CF is the cumulative frequency before the median class
- f is the frequency of the median class
- h is the class interval width

This formulation is widely applied in geophysical studies where measurements are aggregated into intervals.

3. Data Analysis and Results

3.1 TEC

TEC data from five GPS stations (SIET KMITL, MMAI, KMITL Chumphon, NBUA, and PKET) were analyzed to assess ionospheric behavior during Solar cycle 25 (2023-2025). For continuous data acquisition, all stations were equipped with BG2 multi-frequency GPS receivers, covering the low-latitude region of Thailand. TEC datasets were collected directly from GPS observations and compared against global International GNSS Service (IGS) and International Reference Ionosphere (IRI) outputs. These comparisons provided indicators of spatial and temporal consistency while highlighting disparities caused by local ionospheric conditions in Thailand. equatorial ionospheric responses, particularly during peak solar activity as shown in Fig. 3.

In Fig. 3, all TEC data from GPS, IGS, and IRI at five stations are included during the period 2023-2025. The monthly median TEC values derived from GPS, IGS, and IRI across all five Thai stations revealed clear temporal and regional variability linked to Solar cycle 25. The highest GPS TEC values were observed in 2024, with peaks exceeding 100 TECU at northern stations such as MMAI and NBUA, while equatorial Chumphon also exhibited strong responses during solar maxima. In contrast, the lowest values consistently occurred in June 2025, when GPS TEC dropped to 20-35 TECU at several stations, reflecting diminished ionospheric variability as solar activity declined. IGS estimates closely tracked GPS observations, though slightly lower, whereas the IRI model persistently underestimated TEC, particularly during peak equatorial activity. Overall, the results highlight October 2024 as the dominant maximum phase of ionospheric enhancement and June 2025 as the period of minimum activity, underscoring the strong influence of solar flux and regional dynamics on ionospheric electron content in Thailand.

In Fig. 3, the analysis of monthly median TEC values derived from GPS, IGS, and the IRI model for the period 2023-2025 reveals clear seasonal variability across Thailand, as summarized in Table 2. Correlation coefficients were calculated to assess the relationship between GPS and IGS and the IRI. Summary of correlation coefficients (2023-2025) is across all five stations, GPS-IGS correlations remained consistently high, while GPS-IRI correlations were weaker and often unstable. Bangkok (SIET KMITL): GPS/IGS declined from 0.95 (2023) to 0.63 (2025); GPS/IRI stayed low (0.45-0.30). Chiang Mai (MMAI): GPS/IGS stayed strong (0.97-0.83); GPS/IRI dropped from 0.52 (2023) to negative values (-0.08, -0.16). Chumphon (KMITL Chumphon): GPS/IGS peaked at 1.00 in 2024; GPS/IRI fell from 0.65 (2023) to near zero or negative (-0.01, -0.07). Nongbualumphu (NBUA): GPS/IGS nearly perfect (1.00-0.99); GPS/IRI fluctuated from 0.25 (2023) to -0.25 (2025). Phuket (PKET): GPS/IGS perfect in 2023-2024, then 0.86 in 2025; GPS/IRI was moderated and stable (0.41-0.54). In short, GPS/IGS correlations demonstrate strong reliability across all stations. In contrast, GPS/IRI correlations are weaker, variable, and sometimes negative, reflecting limitations of

the IRI model under changing ionospheric conditions. In particular, factors such as the climate and topography of the receiving station, as well as sudden changes such as sunspots and changes in solar activity, are important and include natural changes in the Earth’s magnetic field that may affect TEC.

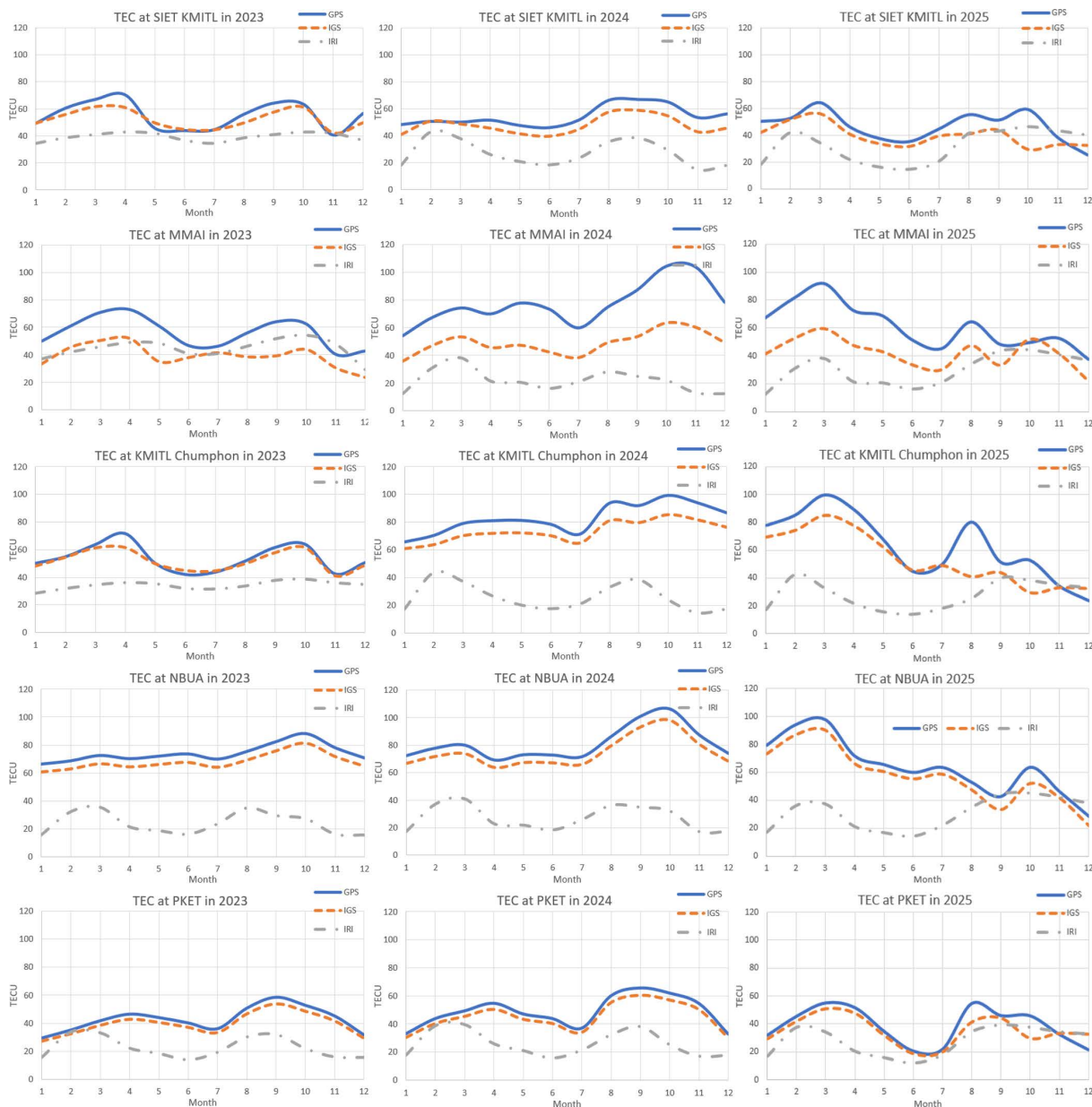


Figure 3. GPS, IGS, and IRI TEC from five stations during the period 2023-2025.

Table 2. Correlation coefficients between (GPS and IGS), (GPS and IRI) at five stations during 2023-2025.

Station	Year	GPS and IGS	GPS and IRI
Bangkok (SIET KMITL)	2023	0.95	0.45
	2024	0.89	0.43
	2025	0.63	0.30
Chiang Mai (MMAI)	2023	0.97	0.52
	2024	0.94	-0.08
	2025	0.83	-0.16
Chumphon (KMITL Chumphon)	2023	0.93	0.65
	2024	1.00	-0.01
	2025	0.85	-0.07
Nongbualumphu (NBUA)	2023	1.00	0.25
	2024	1.00	0.46
	2025	0.99	-0.25
Phuket (PKET)	2023	1.00	0.41
	2024	1.00	0.48
	2025	0.86	0.54

3.2 Time Delay

The time delays were determined by substituting measured TEC from five GPS stations (SIET KMITL, MMAI, KMITL Chumphon, NBUA, and PKET) into the GPS signal delay equation. This method quantitatively assesses the ionospheric effects on GPS signals directly from TEC variations observed during Solar cycle 25 (2023-2025).

Figure 4 shows the monthly GPS latency values from five stations compared to F10.7 cm during Solar cycle 25 (2023-2025) and reveals notable variations in the ionospheric response to solar activity. Each station exhibits distinct temporal patterns, reflecting the complex interplay between solar radiation on the Ionosphere.

At SIET KMITL, the year 2023 demonstrated a faster ionospheric response, with the maximum F10.7 cm value of 161.60 in July corresponding to a shorter time delay (44.56 ns), while the minimum value of 127.30 in December was associated with a longer delay (56.64 ns). In contrast, 2024 showed a delayed response, as the peak flux of 219.60 in August coincided with an extended time delay of 66.11 ns. The year 2025 presented mixed behavior, with both shorter and longer delays observed depending on the period.

At MMAI, the year 2023 indicated a faster response, with the maximum F10.7 cm value of 161.60 in July corresponding to a delay of 46.37 ns, while the minimum value of 127.30 in December was associated with 42.85 ns. In 2024, the peak flux of 219.60 in August coincided with a longer delay of 66.11 ns, whereas the minimum flux of 134.70 in March corresponded to 49.78 ns, reflecting a slower response. In 2025, the maximum flux of 162.25

in September was linked to 48.29 ns, while the minimum of 119.80 in June corresponded to 51.56 ns, suggesting a return to faster delays.

At KMITL Chumphon, the year 2023 showed a faster response, with the maximum flux of 161.60 in July corresponding to 43.69 ns, while the minimum of 127.30 in December was associated with 50.66 ns. In 2024, however, the peak flux of 219.60 in August coincided with a substantially longer delay of 93.86 ns, while the minimum of 134.70 in March corresponded to 79.18 ns, indicating a slower response. In 2025, the maximum flux of 162.25 in September was linked to 51.47 ns, while the minimum of 119.80 in June corresponded to 44.93 ns, again reflecting slower behavior.

At NBUA, the year 2023 did not show a clear reduction in delay, with the maximum flux of 161.60 in July corresponding to 69.80 ns, and the minimum of 127.30 in December associated with 70.60 ns. In 2024, the peak flux of 219.60 in August coincided with a longer delay of 86.51 ns, while the minimum of 134.70 in March corresponded to 80.13 ns, indicating a slower response. In 2025, the maximum flux of 162.25 in September was linked to a shorter delay of 42.68 ns, while the minimum of 119.80 in June corresponded to 59.92 ns, suggesting a faster response.

At PKET, the year 2023 showed a slightly slower response, with the maximum flux of 161.60 in July corresponding to 36.12 ns, while the minimum of 127.30 in December was associated with 31.77 ns. In 2024, the peak flux of 219.60 in August coincided with a shorter delay of 60.07 ns, while the minimum of 134.70 in March corresponded to 49.27 ns



Figure 4. GPS time delay from five stations compared to F10.7 cm during 2023-2025.

TEC Fluctuations and Their Implications for GPS

ns, reflecting a faster response. In 2025, the maximum flux of 162.25 in September was linked to 46.07 ns, while the minimum of 119.80 in June corresponded to 20.46 ns, indicating a pronounced acceleration in ionospheric response.

The analysis of GPS time delays (Fig. 4) provides an assessment of ionospheric effects over Thailand’s low-latitude region during 2023-2025. Monthly TEC data from five stations were converted into signal delays to evaluate temporal variations of individual GPS satellites on an annual basis. The results reveal marked variability linked to sunspot changes and the transition from the declining phase of Solar Cycle 24 to the ascending phase of Solar cycle 25. Overall, the dataset demonstrates how solar activity modulates GPS signals, offering insights for GNSS navigation, satellite performance, and space weather monitoring in Thailand.

The monthly time delay values were analyzed and compared with GPS time delays, IGS results, and IRI estimates. Graphical comparisons demonstrate consistent long-term trends, with GPS and IGS estimates showing close agreement, while IRI consistently underestimated ionospheric delays throughout the study period. For instance, GPS and IGS time delays were highest in early 2024 due to increased solar activity, whereas IRI outputs remained low, reflecting the model’s inability to capture ionospheric variability in Thailand’s equatorial region. Regional differences were also evident: northern stations MMAI and NBUA exhibited strong seasonal persistence, coastal PKET showed greater variability, likely influenced by localized geomagnetic and ionospheric dynamics, SIET KMITL reflected urban equatorial conditions with moderate variability influenced by both solar activity and local atmospheric factors, while KMITL Chumphon displayed pronounced equatorial ionospheric responses, particularly during peak solar activity.

Additionally, graphical comparisons between solar radio flux and GPS TEC from all stations were included to highlight the direct correlation between solar activity and ionospheric electron content. These plots clearly illustrate that increases in F10.7 cm values coincide with enhanced TEC levels, reinforcing the role of solar flux as a primary driver of ionospheric variability across Thailand during Solar cycle 25 (2023-2025). The annual analysis reveals significant variability in GPS time delays, reflecting the progression from the declining phase of Solar Cycle 24 to the ascending phase of Solar cycle 25. Satellites over low-latitude stations, especially Bangkok and Chiang Mai, exhibit enhanced delays during months with elevated TEC due to increased ionization from solar activity. Table 3 summarizes the annual time delay values for each GPS satellite at all five stations from 2023 to 2025, providing a clear overview of inter-satellite and inter-station variability. Overall, the dataset demonstrates how low-latitude GPS signals are modulated by seasonal and solar activity, offering valuable insights for GNSS navigation, satellite performance assessment, and space weather monitoring in Thailand.

Table 3. The summary of each GPS satellite time delay from five stations during 2023-2025.

GPS time delay in 2023-2025 (ns)															
Year	2023					2024					2025				
GPS	SIET KMITL	MMAI	KMITL Chumphon	NBUA	PKET	SIET KMITL	MMAI	KMITL Chumphon	NBUA	PKET	SIET KMITL	MMAI	KMITL Chumphon	NBUA	PKET
G1	13.88	6.16	7.00	–	–	–	0.42	0.00	–	–	13.64	13.55	11.99	8.07	6.42
G2	23.42	27.56	20.32	–	24.96	22.90	18.27	16.43	16.65	14.34	21.15	20.63	14.88	11.12	8.27
G3	28.30	38.60	12.43	–	25.69	23.48	25.98	22.42	12.66	19.16	18.01	7.88	11.83	9.58	6.08
G4	10.93	14.92	13.44	–	42.85	12.90	17.67	26.57	16.60	25.70	11.60	7.04	26.73	13.70	6.52
G5	17.76	19.89	18.92	–	16.76	18.70	42.75	12.80	28.31	8.47	28.05	37.52	26.06	57.56	17.38
G6	8.69	28.03	10.23	–	9.53	28.60	30.19	15.86	30.08	19.11	26.50	37.96	35.96	27.02	24.35
G7	6.98	24.54	55.96	–	16.65	9.26	48.01	44.68	31.22	23.46	13.44	11.26	23.79	13.92	13.74
G8	15.22	49.26	28.92	–	43.29	15.50	35.69	28.45	28.37	40.32	9.08	22.99	16.84	12.23	12.85

GPS time delay in 2023-2025 (ns)															
Year	2023					2024					2025				
GPS	SIET KMITL	MMAI	KMITL Chumphon	NBUA	PKET	SIET KMITL	MMAI	KMITL Chumphon	NBUA	PKET	SIET KMITL	MMAI	KMITL Chumphon	NBUA	PKET
G9	10.41	10.33	15.86	—	10.92	33.22	12.65	36.96	17.11	20.80	15.97	12.14	16.87	7.64	7.12
G10	57.29	44.05	28.37	—	2.93	13.18	41.95	69.80	37.29	13.12	24.77	39.86	84.97	107.49	13.41
G11	10.43	21.61	14.97	—	8.70	18.39	34.01	20.22	18.32	15.93	41.49	62.89	37.59	68.34	18.72
G12	10.21	19.23	18.18	—	6.35	9.47	15.08	16.50	8.88	10.80	24.52	36.87	11.93	32.96	12.00
G13	16.28	14.59	12.33	—	6.48	16.59	27.72	14.93	10.63	15.88	16.58	54.73	14.89	14.54	29.50
G14	43.77	13.68	43.77	—	18.14	56.84	37.12	32.95	77.45	16.68	10.60	16.58	19.12	47.12	17.17
G15	23.87	13.66	23.52	—	10.81	16.15	19.30	22.29	19.54	27.48	16.91	27.17	42.87	24.17	39.82
G16	27.92	27.69	30.80	—	48.02	28.57	23.92	28.22	12.20	25.03	13.99	15.41	8.34	10.86	11.03
G17	21.13	2.16	23.37	—	7.39	23.83	48.40	25.83	33.97	12.73	18.59	23.28	16.73	27.51	10.24
G18	19.52	9.65	32.17	—	6.82	12.14	27.14	45.89	35.59	16.52	8.14	26.90	67.45	45.20	15.62
G19	20.04	13.52	13.32	—	11.14	30.65	49.68	25.98	24.05	13.53	29.34	29.42	20.65	24.49	14.35
G20	16.11	5.23	10.04	—	8.77	16.56	24.90	14.38	12.06	15.84	29.10	17.33	39.81	17.50	31.03
G21	20.82	6.97	15.81	—	23.77	16.44	21.17	23.08	14.12	17.24	1.53	15.76	16.37	15.23	3.98
G22	11.51	9.82	29.95	—	14.52	40.17	44.28	94.09	69.37	15.02	13.73	46.14	121.21	36.47	33.84
G23	28.41	8.60	27.79	—	6.85	30.08	39.55	36.78	51.59	9.83	57.50	38.60	48.46	59.48	10.43
G24	13.37	17.25	8.65	—	6.31	20.37	39.17	16.04	25.45	10.43	12.58	40.22	28.21	38.21	24.21
G25	14.14	3.62	15.87	—	15.86	12.24	25.80	20.43	15.82	11.57	17.30	43.40	37.19	44.57	18.34
G26	34.89	15.43	46.13	—	62.79	16.25	33.89	30.09	30.33	28.16	8.15	46.59	20.91	25.26	13.99
G27	24.20	7.57	39.57	—	46.07	9.12	15.94	16.71	15.22	12.37	14.92	11.31	15.93	13.30	6.29
G28	22.93	6.73	11.90	—	24.64	17.53	41.81	10.19	38.66	8.77	12.64	44.85	8.09	32.56	8.41
G29	17.05	5.11	14.16	—	8.50	11.35	18.46	10.79	13.51	10.67	8.22	18.53	13.44	11.12	10.85
G30	12.84	4.79	9.99	—	31.26	14.46	19.59	22.26	26.95	26.56	21.48	30.78	19.43	23.69	34.46
G31	26.50	4.78	26.96	—	23.51	16.07	30.73	29.26	41.44	11.73	16.24	46.07	17.04	39.50	8.21
G32	33.58	9.70	22.88	—	4.29	30.72	49.05	36.07	44.20	13.12	24.20	61.87	48.96	52.59	7.66

Table 3 shows GPS signal time delays from five stations in Thailand during 2023-2025, reflecting TEC variations linked to Solar cycle 25. In 2023, data from four stations revealed moderate to high delays, with peaks at SIET KMITL (57.29 ns, G10), MMAI (49.26 ns, G8), and KMITL Chumphon (55.96 ns, G7). By 2024, all stations reported increased variability, with notable delays at NBUA (69.37 ns, G22; 51.59 ns, G23) and KMITL Chumphon (69.80 ns, G10). In 2025, delays intensified further, coinciding with the solar maximum, with NBUA recording the highest value (107.49 ns, G10), followed by KMITL Chumphon (84.97 ns, G10) and MMAI (62.89 ns, G11).

Overall, SIET KMITL consistently showed moderate to high delays at northern station at MMAI. NBUA exhibited in trends at northeastern station. Southern station at KMITL Chumphon and PKET displayed episodic spikes. The progressive increase is across all sites underscores the strong influence of solar-induced TEC fluctuations on GPS signal propagation and highlights the need for dynamic ionospheric modeling and real-time monitoring to mitigate navigation errors in low-latitude regions.

4. Discussion

The results indicate that GPS signal delays in Thailand during Solar cycle 25 (2023-2025) were significantly influenced by TEC fluctuations associated with solar activity. GPS and IGS TEC values tracked F10.7 cm flux closely, while the IRI model served only as a climatological background and consistently underestimated TEC. Regional contrasts were evident. Northern stations (MMAI, NBUA) showed stronger seasonal persistence and higher TEC peaks, while coastal PKET exhibited greater variability. KMITL Chumphon, near the magnetic equator, displayed pronounced equatorial responses with extended delays during the 2024 solar maximum. Bangkok (SIET KMITL) reflected moderate variability shaped by both solar activity and local atmospheric factors. The study further confirmed these differences: some stations responded faster in 2023, delays extended in 2024, and mixed or accelerated responses appeared in 2025. Comparisons across GPS, IGS, and IRI datasets extend earlier findings (Kenpankho et al., 2011; Keokhumcheng and Kenpankho, 2025) and align with recent studies (Ansari et al., 2025). The study reinforces that global empirical models often fail to capture localized ionospheric dynamics.

Overall, the study underscores that ionospheric variability in low-latitude regions is both spatially diverse and temporally sensitive to solar cycle phases. These insights support adaptive GPS correction algorithms, integration of real-time space weather monitoring, and expansion of receiver networks critical for GNSS operations in Southeast Asia.

5. Conclusion

This study presents a comprehensive investigation into the impact of solar activity on TEC and GPS signal time delays in the low-latitude region above Thailand during the ascending phase of Solar cycle 25 (2023-2025). Using multi-frequency GPS data from five stations, SIET KMITL, MMAI, KMITL Chumphon, NBUA, and PKET, the analysis reveals significant temporal and spatial variations in ionospheric behavior, closely correlated with sunspots in Solar cycle 25 (2023-2025). The results demonstrate that TEC increases with elevated solar flux, particularly when the F10.7 cm index exceeds 150 sfu. NBUA consistently exhibited the highest TEC values, while PKET recorded the lowest, indicating pronounced regional and latitudinal differences. Comparisons across GPS, IGS, and IRI datasets confirmed that GPS and IGS TEC values maintained strong coherence, while the IRI model was used only as a climatological background reference. This comparison provides contextual understanding of ionospheric variability rather than a direct evaluation of model performance.

Beyond scientific characterization, the observations carry practical implications for GNSS operations in Southeast Asia. Accounting for ionospheric variability is essential to enhance GPS reliability and navigation stability in low-latitude environments where aviation, transportation, and geodetic applications depend on accurate positioning. The findings underscore the importance of developing GPS correction models that integrate localized TEC monitoring and near real-time space weather data. Such models can improve predictive accuracy and provide actionable guidance for aviation safety, transportation planning, and geodetic surveying. Future research should expand receiver networks, integrate near real-time space weather data, and refine ionospheric models to improve spatial resolution and predictive accuracy. These steps will not only strengthen GPS correction strategies but also support policy-level initiatives aimed at ensuring robust GNSS operations across Thailand and the wider Southeast Asian region.

Acknowledgment. The authors would like to express their sincere gratitude to the Space, Satellite, and Study Laboratory (SSS Lab), Department of Engineering Education, School of Industrial Education and Technology, King Mongkut's Institute of Technology Ladkrabang, Bangkok, for providing research equipment and technical support throughout this study. Special thanks are also extended to the Institute of Geology and Geophysics, Chinese Academy of Sciences (IGGCAS), for supplying satellite signal receivers used in data acquisition. The authors acknowledge the Thai Meteorological Department for its support in regional ionospheric data access and appreciate the contributions of the International Reference Ionosphere (IRI) and the International GNSS Service (IGS) for providing global TEC and satellite ephemeris datasets essential to the analysis.

References

- Akala, A. O., O. J. Oyedokun, P. O. Amaechi, K. G. Simi et al. (2021). Solar origins of August 26, 2018, geomagnetic storm: Responses of the interplanetary medium and equatorial/low-latitude ionosphere to the storm, *Space Weather*, 19, e2021SW002734, doi:10.1029/2021SW002734.
- Ansari, K., S. K. Panda, V. Kavutarapu and P. Jamjareegulgarn (2025). Ionospheric gradients in multi-Constellation GNSS signals onboard UAV using GIM and Klobuchar model over Thailand, *Adv. Space Res.*, doi:10.1016/j.asr.2025.07.092.
- Ansari, K., S. K. Panda, V. Kavutarapu and P. Jamjareegulgarn (2024). Towards mitigating the effect of plasma bubbles on GPS positioning accuracy through wavelet transformation over Southeast Asian region, *Adv. Space Res.*, 73, 7, 3642-3657, doi:10.1016/j.asr.2023.04.041.
- Arowolo, O. A., A. O. Akala and E. O. Oyeyemi (2021). Interplanetary origins of some intense geomagnetic storms during solar cycle 24 and the responses of African equatorial/low-latitude ionosphere to them, *J. Geophys. Res. Space Phys.*, 126, e2020JA027929, doi:10.1029/2020JA027929.
- Bilitza, D., M. Pezzopane, V. Truhlik, D. Altadill et al. (2022). The International Reference Ionosphere model: A review and description of an ionospheric benchmark, *Rev. Geophys.*, 60, e2022RG000792, doi:10.1029/2022RG000792.
- Blewitt, G. (1990). An automatic editing algorithm for GPS data, *Geophys. Res. Lett.*, 17, 3, 199-202, doi:10.1029/GL017i003p00199.
- Brajša, R., G. Verbanac, M. Bandić, A. Hanslmeier et al. (2022). A prediction for the 25th solar cycle maximum amplitude, *Astron. Nachr.*, 343, 3, e2113960, doi:10.1002/asna.202113960.
- Chowdhary, V. R., N. K. Tripathi, S. Arunpold and D. K. Raju (2015). Variations of total electron content in the equatorial anomaly region in Thailand, *Adv. Space Res.*, 55, 1, 231-242, doi:10.1016/j.asr.2014.09.024.
- Davies, K. and X. M. Liu (1991). Ionospheric slab thickness in middle and low latitudes, *Radio Sci.*, 26, 4, 997-1005, doi:10.1029/91RS00831.
- Du, Z. (2022). Evolution of the correlation between the amplitude of the solar cycle and the sunspot number since the previous declining phase in both hemispheres, *Sol. Phys.*, 297, 9, 117, doi:10.1007/s11207-022-02051-z.
- Hogg, R. V., J. McKean and A. T. Craig (2005). *Introduction to Mathematical Statistics*, 6th Edition, All Books and Monographs by WMU Authors, 119, <https://scholarworks.wmich.edu/books/119>.
- Javaraiah, J. (2024). Prediction of the amplitude of solar cycle 25 from the ratio of sunspot number to sunspot-group area, low latitude activity and 130 year solar cycle, *Adv. Space Res.*, 74, 3, 1518-1534, doi:10.1016/j.asr.2024.04.043.
- Jesus, R., P. R. Fagundes, A. Coster, O. S. Bolaji et al. (2016). Effects of the intense geomagnetic storm of September-October 2012 on the equatorial, low- and mid-latitude F region in the American and African sector during the unusual 24th solar cycle, *J. Atmos. Sol. Terr. Phys.*, 138-139, 93-105, doi:10.1016/j.jastp.2015.12.015.
- Kalkan, M. Y., D. E. Fawzy and A. T. Saygac (2023). Predictions of solar activity cycles 25 and 26 using nonlinear autoregressive exogenous neural networks, *Monthly Notices of the Royal Astronomical Society*, 523, 4, 4893-4905, doi:10.1093/mnras/stad1460.
- Kenpankho, P., K. Watthanasangmechai, P. Supnithi, T. Tsugawa et al. (2011). Comparison of GPS TEC measurements with IRI TEC prediction at the equatorial latitude station, Chumphon, Thailand, *Earth Planets Space*, 63, 4, 365-370, doi:10.5047/eps.2011.01.010.
- Keokhumcheng, T. and P. Kenpankho (2025). The study of total electron content on ionosphere by using single frequency GPS receiver, *Adv. Space Res.*, 75, 5, 4245-4259, doi:10.1016/j.asr.2024.08.019.
- Lozitsky, V. and V. Efimenko (2023). Early forecast of a maximum in the 25th cycle of solar activity, *Kinemat. Phys. Celest. Bodies*, 39, 45-48, doi:10.3103/s088459132301004x.

- Ma, G. and T. Maruyama (2003). Derivation of TEC and estimation of instrumental biases from GEONET in Japan, *Ann. Geophys.*, 21, 2083-2093, doi:10.5194/angeo-21-2083-2003.
- Mengistu, E., M. B. Moldwin, B. Damtie and M. Nigussie (2019). The performance of IRI-2016 in the African sector of equatorial ionosphere for different geomagnetic conditions and time scales, *J. Atmos. Sol. Terr. Phys.*, 186, 116-138, doi:10.1016/j.jastp.2019.02.006.
- Nagovitsyn, Y. A. and V. G. Ivanov (2023). Solar cycle pairing and prediction of cycle 25, *Sol. Phys.*, 298, 3, 37, doi:10.1007/s11207-023-02121-w.
- NOAA Space Weather Prediction Center. (2024). Daily solar radio flux (F10.7 cm), National Oceanic and Atmospheric Administration, <https://www.swpc.noaa.gov>.
- Oyedokun, O. J., A. O. Akala and E. O. Oyeyemi (2021). Responses of the African equatorial ionization anomaly (EIA) to some selected intense geomagnetic storms during the maximum phase of solar cycle 24, *Adv. Space Res.*, 67, 4, 1222-1243, doi:10.1016/j.asr.2020.11.020.
- Ogwala, A., O. J. Oyedokun, O. Ogunmodimu, A. O. Akala et al. (2022). Longitudinal variations in equatorial ionospheric TEC from GPS, Global Ionosphere Map and International Reference Ionosphere-2016 during the descending and minimum phases of solar cycle 24, *Universe*, 8, 11, 575, doi:10.3390/universe8110575.
- Singh, A., V. S. Rathore, S. Kumar, S. S. Rao et al. (2021). Effect of intense geomagnetic storms on low-latitude TEC during the increasing phase of the solar cycle 24, *J. Astrophys. Astron.*, 42, 2, 99, doi:10.1007/s12036-021-09774-8.
- Tsidu, M. G. and M. M. Zegeye (2020). Comparison of quiet-time ionospheric total electron content from the IRI-2016 model and from gridded and station-level GPS observations, *Ann. Geophys.*, 38, 725-748, doi:10.5194/angeo-38-725-2020.

***CORRESPONDING AUTHOR: Prasert KENPANKHO,**

King Mongkut's Institute of Technology Ladkrabang, Department of Engineering Education,
School of Industrial Education and Technology, Bangkok, Thailand, 10520, Thailand
e-mail: prasert.ke@kmitl.ac.th

© 2026 the Author(s). All rights reserved.

Open Access. This article is licensed under a Creative Commons Attribution 4.0 International